Inorganic Chemistry

Article

pubs.acs.org/IC

On the True Indium Content of In-Filled Skutterudites

Eduard Visnow,[†,▽] Christophe P. Heinrich,[†,‡,▽] Andreas Schmitz,[§] Johannes de Boor,[§] Patrick Leidich,[†] Benedikt Klobes,[⊥] Raphael P. Hermann,[⊥,∥] Wolf Eckhard Müller,[*,§,#] and Wolfgang Tremel[*,†]

[†]Institut für Anorganische Chemie und Analytische Chemie, Johannes Gutenberg-Universität, Duesbergweg 10-14, D-55099 Mainz, Germany

[‡]Graduate School Materials Science in Mainz, Johannes Gutenberg-Universität, Staudinger Weg 9, 55128 Mainz, Germany

[§]Deutsches Zentrum für Luft- und Raumfahrt e.V. (DLR), Institut für Werkstoff-Forschung, Linder Höhe, D-51147 Köln, Germany

[⊥]Jülich Centre for Neutron Science JCNS and Peter Grünberg Institute PGI, JARA-FIT, Forschungszentrum Jülich GmbH, D-52425 Jülich, Germany

[∥]Faculté des Sciences, Université de Liège, B-4000 Liège, Belgium

[#]Institute of Inorganic and Analytical Chemistry, Justus Liebig University Giessen, Heinrich-Buff-Ring 58, D-35392 Giessen, Germany

Supporting Information

ABSTRACT: The incongruently melting single-filled skutterudite $In_xCo_4Sb_{12}$ is known as a promising bulk thermoelectric material. However, the products of current bulk syntheses contain always impurities of InSb, Sb, CoSb, or $CoSb_2$, which prevent an unbiased determination of its thermoelectric properties. We report a new two-step synthesis of high-purity $In_xCo_4Sb_{12}$ with nominal compositions x = 0.12, 0.15, 0.18, and 0.20 that separates the kieftite ($CoSb_3$) formation from the topotactic filler insertion. This approach allows conducting the reactions at lower temperatures with shorter reaction times and circumventing the formation of impurity phases. The synthesis can be extended to other filled skutterudites. High-density (>98%) pellets for thermoelectric characterization were prepared by current-assisted short-time sintering. Sample homogeneity was demonstrated by potential and Seebeck microprobe measurements of the complete pellet surfaces. Synchrotron X-ray diffraction showed a purity of 99.9% product with traces (≤0.1%) of InSb in samples of nominal composition $In_{0.18}Co_4Sb_{12}$ and $In_{0.20}Co_4Sb_{12}$. Rietveld refinements revealed a linear correlation between the true In occupancy and the lattice parameter a. This allows the determination of the true In filling in skutterudites and predicting the In content of unknown $A_xCo_4Sb_{12}$. The high purity of $In_xCo_4Sb_{12}$ allowed studying the transport properties without bias from side phases. A figure of merit close to unity at 420 °C was obtained for a sample of a true composition of $In_{0.160(2)}Co_4Sb_{12}$ (nominal composition $In_{0.18}Co_4Sb_{12}$). The lower degree of In filling has a dramatic effect on the thermoelectric properties as demonstrated by the sample of nominal composition $In_{0.20}Co_4Sb_{12}$. The presence of InSb in amounts of ∼0.1 vol% led to a substantially lower degree of interstitial site filling of 0.144, and the figure of merit zT decreased by 18%, which demonstrates the significance of the true filler atom content in skutterudite materials.

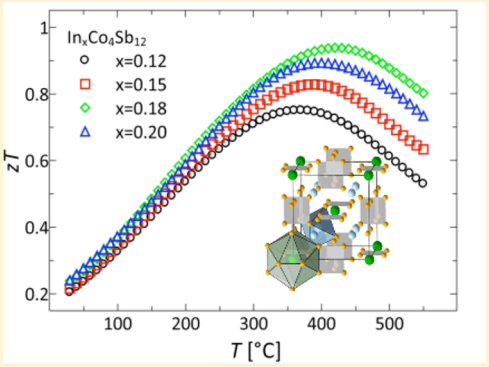

INTRODUCTION

Thermoelectric (TE) materials have been attracting much attention in functional device applications, such as power generators or heat pumps. The devices made from thermoelectric materials should possess the advantage of being highly efficient, environmentally friendly, and inexpensive. The efficiency of a thermoelectric material is usually characterized by its dimensionless figure of merit $zT = (S^2\sigma/\kappa)T$, where S, σ, κ, and T are the Seebeck coefficient, electrical conductivity, thermal conductivity, and absolute temperature, respectively. Good thermoelectric materials should, therefore, be poor thermal conductors and good electrical conductors.[1,2] The key problem is that the electrical transport parameters are interdependent, and attempts to maximize one parameter often have deleterious effects on the other ones. This has limited the figure of merit of commercially available materials to values of about unity, although there is no theoretical limit to the value of zT.

In contrast to the electronic contribution, the lattice thermal conductivity can be altered independently of other transport mechanisms and, therefore, plays a major role in optimizing thermoelectric materials. As a result, there have been significant advances in the development of thermoelectric materials.[3] Enhanced zT values have been reported for superlattices[4,5] and both nanostructured[6−8] and bulk materials.[9−11]

Filled skutterudites appear to have the potential to fulfill all criteria for good thermoelectric materials.[3] These include

Received: April 14, 2015
Published: July 27, 2015

DOI: 10.1021/acs.inorgchem.5b00799
Inorg. Chem. 2015, 54, 7818−7827

inexpensive and abundant constituents, a large unit cell, heavy constituent atom masses, and low electronegativity differences between the constituent atoms. The electrical properties of skutterudite representatives range from metallic or low-temperature superconducting to narrow-gap semiconducting[12,13] with high carrier mobilities.[15] The thermal conductivity of the binary skutterudites is quite high, which leads to low zT values and thus poor conversion efficiency for TE applications.[13−15] However, the complex open structure of cubic skutterudites allows interstitial atoms to be placed into an 20 atom "oversized" cage of the structure, consisting of covalently linked Co and Sb atoms with low charge, as determined by electron density studies. The guest atom exhibits low-energy thermal vibration, which lowers the lattice thermal conductivity.[16−18] In addition, Iversen and co-workers[19,20] investigated partially filled skutterudites with nominal compositions $M_{0.1}(Co_4Sb_{12})$ (M = La, Ce, Nd, Eu, Sm, Yb) by multi-temperature synchrotron powder diffraction. In particular, the exact locations of the defects were studied by combined synchrotron X-ray, neutron, and *ab initio* methods.[21]

As rationalized by the above structural studies filling these 20 atom cages with atoms such as rare-earth,[22−27] alkaline earth,[28−30] alkali,[31,32] and other metals[33−39] proved to be an efficient and general strategy to reduce the lattice part of thermal conductivity by scattering phonons, without impairing the electronic properties.[22,23] In these filled skutterudites,[22−24] the interstitials are only weakly bound to the metalloid Sb atoms, enabling multiple vibrational excitations.[17,18] The concomitant reduction of the lattice thermal conductivity (κ_{lat})[40] leads to a significantly improved zT from 0.5 to 0.8 in doped $CoSb_3$[13] to 1.0−1.1 in (single-element) filled skutterudites[24−33] with the best n-type materials now even reaching zT values between 1.4 and 2.0.[38,39,41,42] Multiple filling,[39,43] nanostructuring[44] or rapid solidification[45] have contributed to these improvements.

Skutterudites are peritectic compounds, which require long annealing times (on the order of several days) for the melt-grown ingots to reach the equilibrium phase. Current synthetic methods rely on melting−quench−annealing,[46] mechanical alloying,[47,48] melt-spinning,[45,49] microwave,[50] high-temperature[44,51] or high-pressure techniques.[52] Due to the peritectic systems mechanical alloying of skutterudites is not as effective as with other thermoelectric systems and often leads to high impurity levels.[53] A particular drawback of the peritectic system is that the sample characteristics strongly depend on the preparation method. $CoSb_3$ melts incongruently at 876 °C.[54] Consolidating a stoichiometric mixture of Co and Sb after heating for 48−62 h at 873−973 °C by hot pressing leads to *n*-type material, whereas *p*-type behavior was observed for cold-pressed samples.[55] In addition, it turned out that $CoSb_{3\pm\delta}$ is not a line phase. The Sb content plays an important role for the chemical behavior and the thermoelectric properties.[56] Similarly, the above-mentioned synthetic routes to In-filled skutterudites $In_xCo_4Sb_{12}$ lead to phase mixtures containing impurities of the side phases InSb, Sb, CoSb, and/or $CoSb_2$, whose effects are apparent in the wide range of reported thermoelectric properties.[57−61] Although larger amounts of nanosized impurities of InSb have been reported to show a beneficial influence on the thermal properties,[44] phase pure samples will facilitate the understanding of structure−property relationships.[62] Besides phase purity, a time-consuming and costly long-term sample annealing constitutes an economical issue. Although a fast microwave synthesis of filled skutterudites was reported recently,[50] the disadvantages concerning phase purity and scalability, which result in materials with inferior thermoelectric properties, are still dominant.

To overcome the problems of long reaction times and material inhomogeneity, we demonstrate a new two-step synthesis of high-performance $In_xCo_4Sb_{12}$ skutterudite bulk material that can easily be expanded to an industrial production level and transferred to other filled skutterudites. By separating the kieftite ($CoSb_{3-\delta}$) host formation from the topotactic filler insertion, the reaction time was dramatically reduced and the formation of side phases circumvented. This allowed an unbiased investigation of the effect of the degree of indium-filling on the structure and the thermoelectric properties. To this end, a series of In-filled skutterudites $In_xCo_4Sb_{12}$ with nominal composition x = 0.12, 0.15, 0.18, and 0.20 were synthesized in bulk quantities. The $In_xCo_4Sb_{12}$ powders were consolidated by current-assisted short-time sintering. The thermal stability, structural, and microstructural properties of the powders and sintered pellets were investigated. The excellent sample homogeneity was demonstrated via scanning electron microscopy (SEM) combined with energy-dispersive X-ray spectroscopy (EDX), potential and Seebeck microprobe (PSM) measurements, ^{121}Sb Mößbauer spectroscopy, and powder X-ray diffraction (XRD) of standard laboratory and synchrotron data. Rietveld refinements revealed a marginal volume fraction of InSb in few samples and allowed to determine the actual degree of In filling and to correlate it with the thermoelectric transport data. Our results also allow predicting the In content of unknown compounds $In_xCo_4Sb_{12}$. In essence, the In filling has a beneficial effect on both electronic and thermal properties, and the zT could be increased up to a value close to unity at 420 °C. A minor amount of InSb (∼0.1 vol%) in some samples had no significant effect on the transport properties; however, the associated lower actual degree of In filling had a dramatic effect on the thermoelectric properties. It resulted in an up to 18% reduction of zT, which illustrates the importance of the extent of interstitial site occupancy in skutterudite-type materials.

EXPERIMENTAL SECTION

Synthesis. Bulk samples of polycrystalline $In_xCo_4Sb_{12}$ with x = 0, 0.12, 0.15, 0.18, and 0.20 were prepared by solid-state reactions in dried evacuated quartz ampules of 11 mm inner diameter using elemental powders of In (Alfa Aesar, 99.999%), Co (Alfa Aesar, 99.998%), and Sb shots (Alfa Aesar, 99.9999%). The phase purity of all starting materials was verified by XRD, and all synthetic procedures were carried out under controlled atmosphere in a N_2 glovebox. Annealing was performed in evacuated quartz ampules, which were preheated at 800 °C under dynamic vacuum for 5 h to ensure dry conditions. In the first step, the starting elements (∼5 g) were thoroughly ground, sealed in quartz ampules (10 cm length), and annealed at 700 °C for 12 h. During this initial reaction, the $CoSb_3$ phase was formed. To eliminate small amounts of excess Sb, the compact powder (∼5 g) was finely ground and re-annealed in quartz ampules (20 cm length) at 700 °C for 12 h. During the annealing step, excess Sb transports to the opposite side of the ampule, driven by the natural temperature gradient within a horizontal tube furnace. In the final step, phase-pure $CoSb_{3-\delta}$ was thoroughly mixed with In, sealed again in a quartz tube, and reacted at 700 °C for 48 h. The heating and cooling rates for all procedures in the horizontal tube furnace were 5 K/min. The obtained powders of $In_xCo_4Sb_{12}$ were manually ground, and phase purity was verified by standard XRD prior to further processing.

Powder Processing. Batches of bulk powders with different In content were used for consolidation into 1−1.5 mm thick, 12.7 mm

DOI: 10.1021/acs.inorgchem.5b00799
Inorg. Chem. 2015, 54, 7818−7827

diameter disks at 590 °C under a pressure of 56 MPa by direct current-assisted short-time sintering. Boron nitride-coated high-density graphite was used as die material to sinter four pellets simultaneously in the same die. The heating rate was ~60 K/min. Maximum temperature and pressure were applied for 10 min before the pressure was released, and the sample cooled down in an uncontrolled manner. The resulting pellets had a theoretical density >98% as determined by the pellet mass and the Archimedes method.

Sample Characterization. *Room-Temperature Powder X-ray Diffraction (XRD).* Analysis was performed on a Siemens D5000 powder diffractometer in transmission geometry with a Braun M50 position-sensitive detector, Ge (220) monochromator, and Cu Kα radiation, with a step size of 0.0078° in 2θ. The samples were mounted between two strips of 3M Scotch tape.

High-Resolution Synchrotron Powder Diffraction. Data were collected on beamline 11-BM at the Advanced Photon Source (APS) of the Argonne National Laboratory (ANL) with an average wavelength of 0.413721 Å. Discrete detectors covering an angular range from −6° to 16° in 2θ were scanned over a 34° 2θ range, with data points collected every 0.001°θ and a scan speed of 0.01°/s. All samples were diluted with amorphous silica in a 1:1 molar ratio to reduce the X-ray absorption and to obtain a total $\mu R \approx 1$ (where μ is the absorption coefficient and R is the capillary radius). The samples were mounted in Kapton tubes with radii of 0.4 mm. Rietveld refinements of all diffraction data were performed with Topas Academic V4.1[63] applying the fundamental parameter approach.[64]

Scanning Electron Microscopy (SEM) Images and Energy-Dispersive X-ray Spectroscopy (EDX). SEM and EDS measurementsof the as-synthesized powders and the sintered pellets were recorded using a FEI Nova NanoSEM600 equipped with an Everhart−Thornley detector (ETD) and a low-voltage, high-contrast detector (vCD) in high-vacuum mode. The acceleration voltage was chosen to be between 15 and 30 kV. The samples were mounted on an aluminum stub using adhesive conductive carbon tape. For EDX, a built-in EDAX-Genesis detector was used.

Thermoelectric Characterization. Thermoelectric characterization was conducted at the German Aerospace Center (DLR). Temperature-dependent Seebeck coefficients and electric conductivities were measured simultaneously on the HT-S-σ2 measuring system (high-temperature Seebeck & electrical conductivity).[65,66] Thermal diffusivity was measured on a Netzsch laser flash diffusivity instrument (LFA 427). Heat capacity (C_p) was estimated using the Dulong−Petit approximation (C_p = 3 kB per atom), and theoretical densities were calculated from the molar mass and the refined lattice parameters for each composition. The accuracy of measurements was estimated to be 5%, 7%, and 10% for the Seebeck coefficient, the electrical conductivity, and the thermal conductivity, respectively.[60] Homogeneity of the sintered samples was studied utilizing the potential and Seebeck microprobe (PSM)[67] for scanning the local distribution of room-temperature Seebeck coefficients on both sides of the polished pellets. The step size was set to 100 μm, resulting in approximately 10 000 measurement points on each side of the samples.

^{121}Sb Mößbauer Measurements. were performed in standard transmission geometry using a $Ca^{121m}SnO_3$ source with nominal activity of 0.3 mCi and a constant acceleration spectrometer. During the measurements, samples were held 10 K in order to increase the fraction of recoil-free emission and absorption processes. The velocity calibration was performed with α-Fe at room temperature utilizing a ^{57}Co/Rh source. The extracted isomer shifts are reported in reference to InSb at 10 K (δ = −8.6 mm/s relative to the $Ca^{121m}SnO_3$ source).

RESULTS AND DISCUSSION

Synthesis. In a standard route to the incongruently melting $CoSb_3$, a mixture of the elements is heated to temperatures above the melting point (T_m) and quenched rapidly to room temperature to minimize, but not complete exclude, phase decomposition above the decomposition temperature (T_d).[68] The addition of In as a filler element leads to the reaction with formed Sb side phase to InSb as an impurity phase.

In order to avoid long annealing times and the formation of binary In−Sb side phases, the synthesis was divided into two steps. In the first step, single phase $CoSb_3$ was synthesized by reacting Co and Sb powder for 12 h at 700 °C. This reaction temperature is well below the decomposition temperature of $CoSb_3$, but still above the melting point of Sb, which results in a minimum reaction time of 10 h. Although the reaction occurs above the melting point of Sb, a reaction of Co dissolved in a Sb melt can be excluded, because no molten beads were formed. The product consists of a compact powder. A reaction involving the gas phase, however, cannot be excluded. Traces of remaining Sb were removed in a purification step by "sublimation−condensation" in the natural temperature gradient of the tube furnace. Optimization studies revealed that the purification can be complete after only 3 h, as indicated by the absence of X-ray intensities of Sb. It is unclear whether the transported Sb arises from traces of unreacted educt (below the detection limit of the laboratory XRD), or whether the antimony leaks out of already formed kieftite ($CoSb_3$) phase. A quantification of the Sb defect concentration in the resulting $CoSb_3$ proved impossible.

In the second step, the kieftite powder was thoroughly mixed with indium, sealed again in an ampule and reacted for 48 h at 700 °C. A set of bulk powder batches with different In contents ($In_xCo_4Sb_{12}$, with x = 0.12, 0.15, 0.18, and 0.20) was made to investigate the phase composition, the homogeneity, and the effect of the filling level on the thermal and electronic transport properties. To ensure sample homogeneity and reproducibility of all measurements, several samples of each compound were synthesized and merged to form large batches. Phase purity was confirmed by powder XRD and Rietveld refinements.

SEM/EDX Analysis. Exemplary scanning electron microscopy images of the synthesized powders and consolidated/measured pellets are shown in Figure 1. Samples with varying

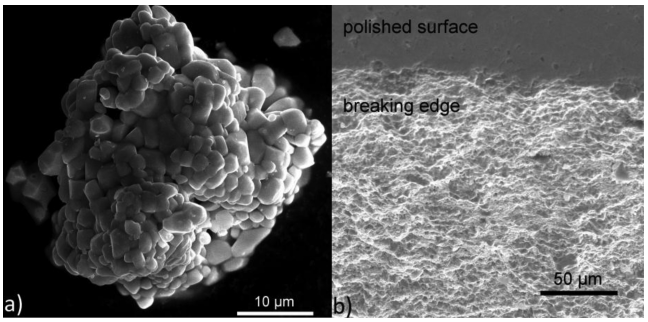

Figure 1. SEM image of $In_xCo_4Sb_{12}$ bulk powder (a) and consolidated $In_xCo_4Sb_{12}$ pellet (b). No significant grain growth took place during the short-time sintering process and the thermal cycling due to thermoelectric characterization. Images were taken from a sample of nominal composition $In_{0.12}Co_4Sb_{12}$.

In content did not exhibit any differences with respect to the sample homogeneity, grain size distribution or grain growth during the sintering process. The surface of the powder (Figure 1a) and the polished surface of the pellet (top part Figure 1b) show no signs of contrast, indicating good material homogeneity. The two step synthesis therefore seems to be better suited for the preparation of phase pure materials than the melt-quench-anneal method, which is known to lead to side phases of Sb and InSb at the grain boundaries.[60]

The polished surface and the breaking edge of the pellet (Figure 1b) show only a few cavities, confirming the high

DOI: 10.1021/acs.inorgchem.5b00799
Inorg. Chem. 2015, 54, 7818−7827

density obtained by current-assisted short-time sintering. The grain sizes before and after consolidation range from 2 to 5 μm, which demonstrates the absence of significant grain growth during the sintering process and even several subsequent thermal cycles of thermoelectric characterizations.

Potential and Seebeck Microprobe (PSM). To underline the homogeneous In intercalation a PSM characterization was performed on all samples. The Seebeck coefficient is very sensitive to compositional changes, which affect the charge carrier concentration. An inhomogeneous distribution, either of In as a filler atom or of Sb defects, would result in a significant change of the Seebeck coefficient. Figure 2 shows a typical plot

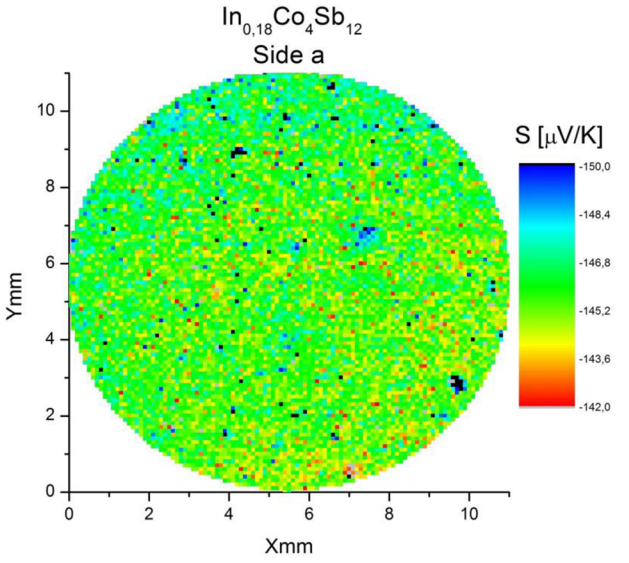

Figure 2. Potential and Seebeck microprobe measurement of the complete face of a consolidated pellet of nominal composition $In_{0.18}Co_4Sb_{12}$. The very uniform and narrow distribution of Seebeck values demonstrates the outstanding sample homogeneity obtained by the two-step synthesis method.

of the PSM measurements obtained from the complete pellet base face. The sample of nominal composition $In_{0.18}Co_4Sb_{12}$ provides information on the range of obtained Seebeck values in the pellet and demonstrates excellent sample homogeneity. Figure S1 (Supporting Information) illustrates the obtained Seebeck distribution measured on both sides of all samples. The individual measurements show a small distribution of Seebeck coefficients <20 μV/K (Figures S2–S8), which underlines the good sample homogeneity. Very small difference can be observed between measurements operated on opposite sides of some of the pellets. This might indicate a slight compositional gradient along the pellet height, possibly resulting from a temperature gradient, due to the Peltier effect, during the sintering process. However, these differences of 5 μV/K are very subtle and do not significantly affect the thermoelectric figure of merit.[69]

^{121}Sb Mößbauer Spectroscopy. Mößbauer spectroscopy allows the detection of subtle changes in nuclear energy levels, which are triggered by the chemical environment of the nucleus (e.g., oxidation state, bonding properties, etc.). ^{121}Sb Mößbauer spectra were recorded to obtain more information concerning the presence of InSb as a side phase and Sb deficiencies or In substitution on the Sb lattice sites that might make a detectable difference on the environment of Sb at the 24g Wyckoff site. To this end, a set of skutterudite samples with the compositions $In_{0.12}Co_4Sb_{12}$ and $In_{0.2}Co_4Sb_{12}$ were measured before and after consolidation and thermal cycling, and subsequently compared to the ^{121}Sb Mößbauer spectrum of an unfilled kieftite sample. The Mößbauer spectrum obtained from the $In_{0.2}Co_4Sb_{12}$ sample after consolidation and thermal cycling is shown in Table 1 and Figures S9–S13. The isomer shifts relative to InSb

Table 1. Isomer Shift, Quadrupole Splitting, Asymmetry Parameter, and Line Width of the ^{121}Sb Mößbauer Spectra

sample	isomer shift (mm/s)	quadrupole splitting (mm/s)	asymmetry parameter	line width (mm/s)
$CoSb_3$	−0.9(1)	9.6(6)	0.8(2)	3.8(3)
$In_{0.12}Co_4Sb_{12}$	−1.0(1)	9.8(7)	1.0(2)	3.7(3)
$In_{0.15}Co_4Sb_{12}$	−1.1(1)	9.0(3)	0.8(1)	3.1(1)
$In_{0.18}Co_4Sb_{12}$	−1.2(1)	11.6(7)	0.6(3)	3.5(4)
$In_{0.20}Co_4Sb_{12}$	−1.0(1)	9.2(1)	0.8(1)	3.0(1)

and quadrupole splitting correspond well to published $CoSb_3$ data.[66,70−72] The presence of a small InSb side phase concentration in $In_{0.2}Co_4Sb_{12}$ samples, demonstrated by high-resolution synchrotron XRD (*vide infra*), and thermal cycling (comparison between powder and pellet samples) is well below the detection limit (about 0.5%) of ^{121}Sb Mößbauer spectroscopy.

Powder X-ray Diffraction. The phase purity of all samples was analyzed by laboratory XRD before and after powder consolidation. Still, some questions concerning site occupancies or possible anti-site disorder could not be answered due to the limited resolution and weak, but significant, sample fluorescence. To this end, high-resolution synchrotron diffraction data were collected for a set of eight samples, comprising unprocessed powders of compositions $In_xCo_4Sb_{12}$ (x = 0.12, 0.15, 0.18, and 0.20) and also $In_{0.12}Co_4Sb_{12}$ samples after consolidation and first, second, and third cycles of thermoelectric characterization, at beamline 11-BM at the Advanced Photon Source (APS) of the Argonne National Laboratory (ANL). This set of samples was chosen to study the effect of the indium site occupancy on the structure. The data obtained from 11-BM generally has the advantage of high resolution (<0.0002 $\Delta Q/Q$), no sample fluorescence, and low sample absorption. The energy of the Sb L edge is just below the energy of ∼30 keV used at 11-BM, which results in a total sample absorption of ∼2.8 μR. Normally, measurements of samples up to a total absorption value of 5 μR are considered suitable, if absorption is accounted for during Rietveld refinement. In order to obtain data sets without any significant contribution of absorption, all samples were diluted with amorphous silica in a 1:1 molar ratio.[73]

Occupancy parameters were refined in separate least-squares cycles with a fixed scale factor in alternation with the thermal parameters until convergence to check for deviations from the ideal occupancies. In addition, several refinement cycles were conducted to implement possible anti-site disorder of In and Sb.[73] Large errors in site occupancies and temperature parameters (B_{iso}) combined with too high or low B_{iso} values indicated an over-parameterization, and therefore the final refinements cycles were performed using a structure model assuming the absence of anti-site disorder. In order to accurately determine possible anti-site disorder neutron diffraction or combined neutron/synchrotron diffraction data would be required.

DOI: 10.1021/acs.inorgchem.5b00799
Inorg. Chem. 2015, 54, 7818−7827

Diffraction patterns for $In_{0.12}Co_4Sb_{12}$ and $In_{0.20}Co_4Sb_{12}$ are shown in Figure 3, including profiles, profile fits, and profile differences. The complete set of refined synchrotron data is supplied in the Supporting Information (Tables S1 and S2, Figures S14 and S15). The refined data clearly demonstrate the high quality (phase purity and crystallinity) of the filled skutterudite materials obtained by the two-step method. Although the samples exhibit quite different thermoelectric properties (*vide infra*), the differences in the powder patterns are difficult to determine at a glance. Only the extreme enlargement of the figures (see zoomed-in insets in Figure 3) showed very subtle, additional Bragg intensities, marked by an asterisk, for the two samples of highest nominal In content, $In_{0.18}Co_4Sb_{12}$ (Figure S15) and $In_{0.20}Co_4Sb_{12}$ (Figure 3b). This additional phase can be indexed to cubic InSb, indicated by the lower tick marks in Figure 3b. These additional reflections could only be detected due to the high spatial resolution and beam flux at beamline 11-BM. They could not be resolved by standard laboratory powder diffraction. The marked reflection of InSb at $Q \approx 2.75$ Å^{-1} corresponds to the second strongest (80%) (220) Bragg intensity of the InSb diffraction pattern. Note that the absolute intensity after background subtraction is still below 100 counts.

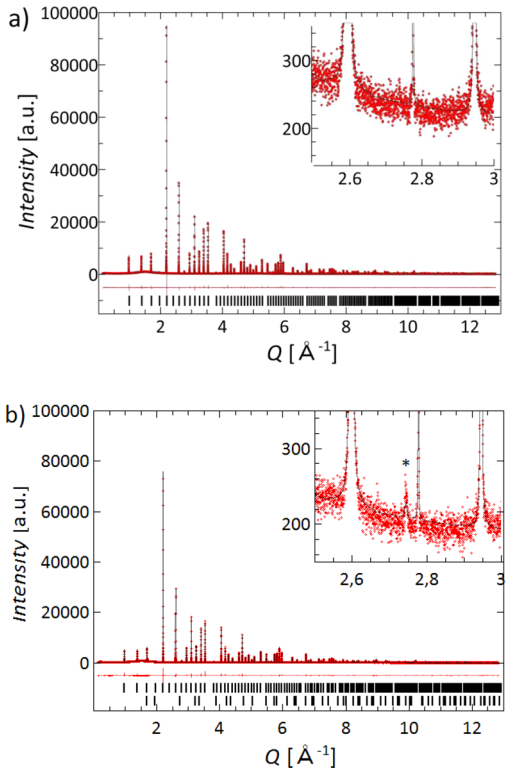

Figure 3. Refined powder diffraction data for samples of nominal composition $In_{0.12}Co_4Sb_{12}$ (a) and $In_{0.20}Co_4Sb_{12}$ (b), including profile fit (black solid line) and profile difference (red solid line). The refined peak positions are indicated by black tick marks. The zoomed-in plots illustrate the presence of InSb as side phase marked by an asterisk in the $In_{0.20}Co_4Sb_{12}$ diffraction pattern. Note the large difference in peak intensities between the skutterudite and the InSb side phase.

In comparison, the strongest skutterudite Bragg intensity has more than 70000 counts, which illustrates that the impurity phase represents only a very small volume fraction of the sample. However, due to the weakness of the reflections a full quantitative analysis is not possible, and the refined value of ~0.1 vol% has to be taken as an estimate. Two very broad reflections in every plot around Q = 1.5 and 5 Å^{-1} show the contribution of the amorphous silica. In order to allow a proper background evaluation, these intensities were modeled via "dummy" reflections prior to the refinement.

For further evaluation, refined parameters such as the lattice parameter a, y- and z-coordinates of the 24g Sb site, vol% of InSb side phase, site occupancies, and isotropic atomic thermal parameters (B_{iso}) of In, Co, and Sb are listed in Tables 2 and 3. The weighted profile residuals and goodness of fit for all refinements are below 6.7% and 1.1, respectively. Due to sample contamination during sample preparation for synchrotron measurements the sample with nominal composition $In_{0.15}Co_4Sb_{12}$ turned out to have larger estimated standard deviation values. In Figure 4, the refined In site occupancy is plotted against the refined lattice parameter. The linear trend illustrates the increase of the lattice parameter due to the expansion of the unit cell, which is a direct consequence of filling the crystallographic void. The refined values are in excellent agreement with results from other reports.[54,56,57,74,75,76] Figure S16 compares the lattice parameter derived from the refined degree of In filling with the data provided by He et al.[57] It is important to note that samples with a nominal In content of x = 0.18 and 0.20 have a substantially lower "true" degree of In filling due to the formation of (minor amounts of) InSb. The In occupancy for the sample of nominal composition $In_{0.20}Co_4Sb_{12}$ is reduced by almost 28% to a value of 0.144, which is even lower than the value of 0.160 refined for the sample of nominal composition $In_{0.18}Co_4Sb_{12}$. Therefore, the formation of InSb plays a crucial role for the true In occupancy, which can be understood considering the very different In contents for $In_xCo_4Sb_{12}$ and InSb. The other refined parameters showed no significant trends. Co and Sb have a full site occupation, and the refined isotropic atomic temperature factors for In, Co, and Sb were in good agreement with comparable literature values.[48,70] The large calculated isotropic thermal parameters of In illustrate the rattling character of the filler atom, which is typical for filled skutterudites.

The refinements of the synchrotron diffraction data of the $In_{0.12}Co_4Sb_{12}$ samples after consolidation and several cycles of

Table 2. Refined Weighted Profile Residual (R_{wp}), Goodness of Fit (GOF), Lattice Parameter a, y- and z-Coordinates of Sb, and Contents (vol%) of the InSb Side Phase[a]

sample	R_{wp} [%]	GOF	LP [Å]	y-coord. (Sb)	z-coord. (Sb)	InSb [vol%]
$In_{0.12}Co_4Sb_{12}$	0.05896	1.104	9.04615(0)	0.15798(2)	0.33525(2)	0
$In_{0.15}Co_4Sb_{12}$	0.09063	1.373	9.04756(0)	0.15836(5)	0.3353(5)	0
$In_{0.18}Co_4Sb_{12}$	0.06574	1.052	9.05078(0)	0.15788(3)	0.3351(3)	0.087(18)
$In_{0.20}Co_4Sb_{12}$	0.06627	1.066	9.04958(0)	0.15779(3)	0.33498(3)	0.116(20)

[a]Numbers in parentheses indicate the estimated standard deviation determined from the refinement.

DOI: 10.1021/acs.inorgchem.5b00799
Inorg. Chem. 2015, 54, 7818−7827

Table 3. Refined Site Occupancies (Occ) and Isotropic Atomic Temperature Factors (B_{iso}) of In, Co, and Sb[a]

	Occ [%]			B_{iso} [Å^2]		
sample	In	Co	Sb	In	Co	Sb
$In_{0.12}Co_4Sb_{12}$	0.113(2)	1.000(1)	1.000(1)	1.83(13)	0.28(7)	0.482(2)
$In_{0.15}Co_4Sb_{12}$	0.111(3)	1.003(3)	0.985(3)	1.78(26)	0.28(1)	0.470(5)
$In_{0.18}Co_4Sb_{12}$	0.160(2)	1.009(2)	1.000(1)	3.00(13)	0.37(8)	0.463(3)
$In_{0.20}Co_4Sb_{12}$	0.144(2)	1.005(1)	1.000(1)	1.63(12)	0.28(8)	0.442(3)

[a]Numbers in parentheses indicate the estimated standard deviation determined from the refinement.

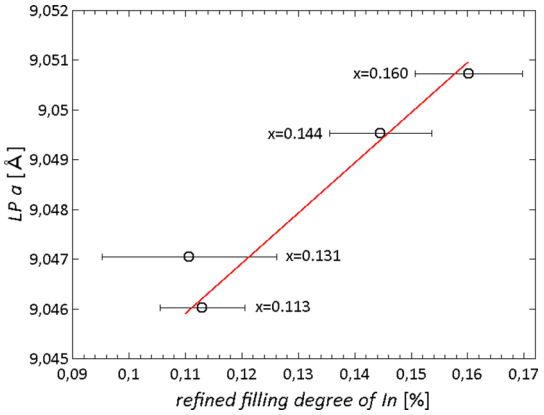

Figure 4. Refined In site occupancy plotted against the lattice parameter *a*. The true compositions of the samples were refined for the samples with nominal compositions x = 0.12, 0.18, and 0.20, the sample with nominal x = 0.15 is calculated from the linear fit of other three samples. Lower filling degree of indium can be explained by different InSb contents, which reduce the amount of In occupying the void site.

thermoelectric characterization show a convergent decrease of the lattice constant (Figure 5), which is currently under investigation. Loss of In caused by the heat treatment may limit the use of skutterudite type materials for power generation to temperatures <500 °C.

Thermoelectric Properties of In-Filled Skutterudites. The temperature-dependent electrical conductivity and Seebeck coefficient of the In-filled skutterudites $In_xCo_4Sb_{12}$ (x = 0.12, 0.15, 0.18, and 0.20) between room temperature and 550 °C are shown in Figure 6.

The electrical conductivity data collected during heating are slightly higher than those measured during cooling. However, above 500 °C the conductivity data converge, which might also indicate some sample degradation at elevated temperatures. The loss of charge carriers due to a decreasing In content (as

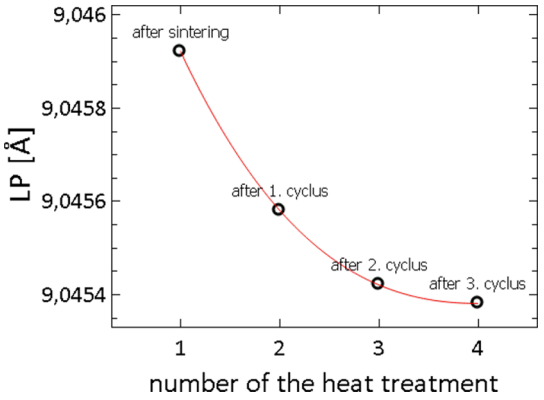

Figure 5. Refined lattice parameter of the $In_{0.12}Co_4Sb_{12}$ samples plotted against the number of heat treatments. The first heat treatment corresponds to the consolidation of the powder; the other three steps correspond to cycles of the thermoelectric characterization. The corresponding In contents extracted from the lattice constant *a* are 0.1192, 0.1164, 0.1150, and 0.1148.

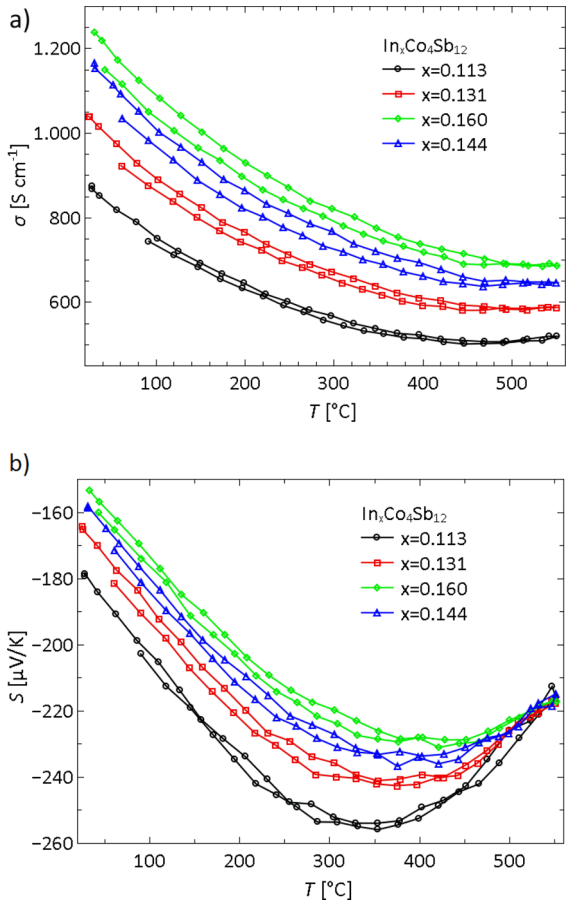

Figure 6. Temperature dependence of the electrical conductivity (a) and Seebeck coefficient (b) from the degree of In filling for the nominal $In_xCo_4Sb_{12}$ (x = 0.12, 0.15, 0.18, and 0.20) and the true composition $In_xCo_4Sb_{12}$ (x = 0.113, 0.131, 0.160, and 0.144), illustrating the correlation of increasing charge carrier concentration with the degree of In filling. The true compositions of the samples were refined for the samples with nominal compositions x = 0.12, 0.18, and 0.20. The sample with nominal x = 0.15 was calculated from the linear fit of other three samples. The electrical conductivity and Seebeck coefficient are increased and decreased, respectively, with increased charge carrier concentration. The heating (the upper graphs) and cooling data (the lower graphs) show a decrease of the electrical conductivity and increase of the absolute Seebeck coefficient upon thermal cycling.

DOI: 10.1021/acs.inorgchem.5b00799
Inorg. Chem. 2015, 54, 7818−7827

demonstrated by synchrotron data collected after measurement cycles of $In_{0.12}Co_4Sb_{12}$) may explain this effect. All measured In filled skutterudites exhibit an electrical conductivity >500 S/cm over the complete temperature range. It decreases slightly with increasing temperature, as expected for heavily doped semiconductors, and it increases with the degree of In filling due to the electron donating nature of the In filler atom. A higher filling level it results in a higher charge carrier concentration and, thus, in a higher electrical conductivity. The sample of nominal composition $In_{0.18}Co_4Sb_{12}$ (highest true degree of In filling) exhibits the highest electrical conductivity of 1250 S/cm at room temperature and 700 S/cm at 550 °C.

All In-filled skutterudites exhibit a large negative Seebeck coefficient, which indicates electrons to be the majority charge carriers. The decrease in Seebeck coefficient above a certain temperature can be explained by the contribution of bipolar conduction, resulting from thermal excitations of electrons over the band gap and the resulting holes in the valence band. Similar to the electrical conductivity, the Seebeck coefficient scales with the degree of In filling. At high temperature, intrinsic charge carriers become dominant due to thermal excitations across the band gap, which results in similar values of the Seebeck coefficients above 500 °C. Analogous to the electrical conductivity, a slight difference between the data collected during heating and cooling could be observed for some samples.

The high electrical conductivity and absolute Seebeck coefficient of the In-filled skutterudites $In_xCo_4Sb_{12}$ (x = 0.12, 0.15, 0.18, and 0.20) lead to excellent values for the power factor $S^2\sigma$ shown in Figure 7. The power factor increases with

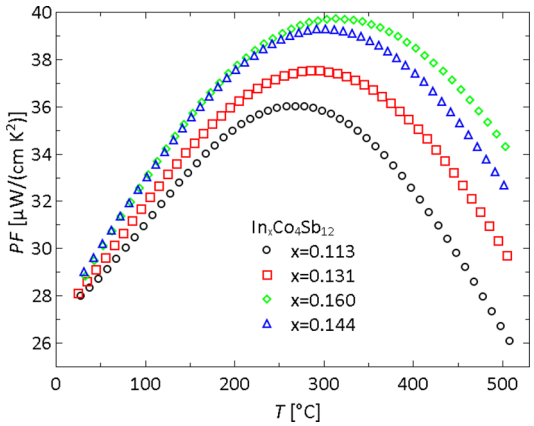

Figure 7. Temperature dependence of the power factor (PF) from the degree for the nominal $In_xCo_4Sb_{12}$ (x = 0.12, 0.15, 0.18, and 0.20) and the true composition $In_xCo_4Sb_{12}$ (x = 0.113, 0.131, 0.160, and 0.144), illustrating the correlation of increasing charge carrier concentration with the degree of In filling. The true compositions of the samples were refined for the samples with nominal compositions x = 0.12, 0.18, and 0.20. The sample with nominal x = 0.15 was calculated from the linear fit of other three samples, illustrating an enhanced power factor with increasing indium-filling degree.

increasing temperature, due to the increase of the absolute value of the Seebeck coefficient, at lower temperatures and reaches a maximum at ~300 °C, with values ranging from 35 to 39 μW cm^{-1} K^{-2}. The sample of nominal composition $In_{0.18}Co_4Sb_{12}$ (highest true degree of In filling) exhibits the highest power factor.

The In filling has not only a beneficial effect on the electronic properties, it also leads to a dramatic reduction in the thermal conductivity. Figure 8 shows the total thermal and lattice

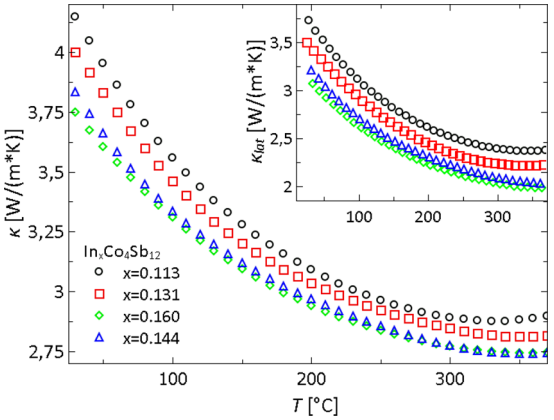

Figure 8. Dependence of the total (the external graph) and lattice (the inner graph) thermal conductivity on the indium-filling degree of skutterudite samples with the nominal $In_xCo_4Sb_{12}$ (x = 0.12, 0.15, 0.18, and 0.20) and the true composition $In_xCo_4Sb_{12}$ (x = 0.113, 0.131, 0.160, and 0.144). The true compositions of the samples were refined for the samples with nominal compositions x = 0.12, 0.18, and 0.20. The sample with nominal x = 0.15 was calculated from the linear fit of other three samples. With increasing true indium-filling degree the electronic thermal conductivity is increased, whereas the lattice thermal conductivity is reduced.

thermal conductivity for $In_xCo_4Sb_{12}$ (x = 0.12, 0.15, 0.18, and 0.20) between 25 and 350 °C. Compared to binary kieftite, which has a thermal conductivity of ~11 W K^{-1} m^{-1} at room temperature, the thermal conductivity of all In-filled skutterudites is greatly reduced. The differences in the thermal conductivity among the set of In filled samples are less pronounced, however, with increasing filling degree the thermal conductivity is lowered from values between 4.15 and 3.75 W K^{-1} m^{-1} at room temperature to minimum values between 2.88 and 2.75 W K^{-1} m^{-1} around 350 °C. Above 350 °C the thermal conductivity increases again due to incipient bipolar conduction. (Figure S19) The effect of In filling on the thermal conductivity can be assessed by separating the electronic and lattice contributions to the thermal conductivity. (Figures S17 and S18) The temperature-dependent electronic contribution was estimated using single parabolic band model and the heating values from electrical conductivity and Seebeck coefficient. At room temperature, the electronic thermal conductivity κ_{el} increases from 0.53 to 0.75 W K^{-1} m^{-1} with increasing In filling. In contrast, the room-temperature lattice thermal conductivity κ_{lat} decreases from 3.62 to 3.00 W K^{-1} m^{-1} with increasing actual In filling level. This trend can easily be explained by the properties of In as filler atom. When an In atom occupies the crystallographic void of the skutterudite structure, the filler atom is only weakly bound to the host structure. In result, the lattice thermal conductivity is lowered, due to the addition of low energy eigenmodes to the phonon spectrum of the host lattice. In addition, these indium atoms are also capable of donating electrons to the $CoSb_3$ host, which in turn increases the charge carrier concentration and the electrical conductivity, thereby leading to an increase of the electronic contribution to the thermal conductivity.

The increasing amount of InSb in the samples of nominal composition $In_{0.18}Co_4Sb_{12}$ and $In_{0.20}Co_4Sb_{12}$ appears to have no

DOI: 10.1021/acs.inorgchem.5b00799
Inorg. Chem. 2015, 54, 7818−7827

effect on the lattice thermal conductivity, which scales solely with the increasing degree of In filling. This might be correlated to their only marginal presence or could indicate that InSb precipitates do not reduce the lattice thermal conductivity.[44,60] The great potential of phonon engineering in skutterudite-type materials is documented by the fact that the lattice thermal conductivity is responsible for the major contribution to the total thermal conductivity. A further reduction of the lattice thermal conductivity, e.g. by multiple filler atoms, enhanced grain boundary scattering or point defect scattering, should thus have a great effect on the thermoelectric figure of merit zT.

The figure of merit for $In_xCo_4Sb_{12}$ (x = 0.12, 0.15, 0.18, and 0.20) was calculated by combining the electronic and thermal contribution to the thermoelectric properties (see Figure 9). At

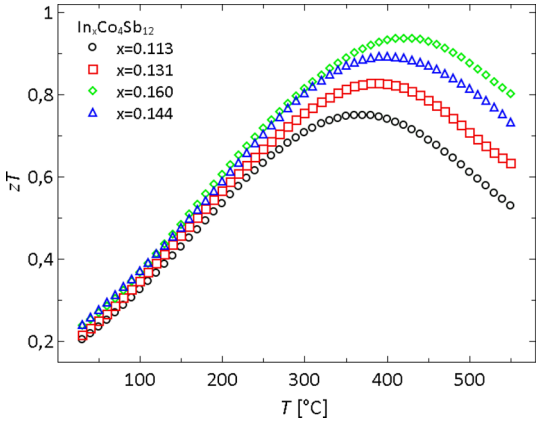

Figure 9. Temperature dependence of the thermoelectric figure of merit as a function of the degree for the nominal $In_xCo_4Sb_{12}$ (x = 0.12, 0.15, 0.18, and 0.20) and the true composition $In_xCo_4Sb_{12}$ (x = 0.113, 0.131, 0.160, and 0.144). The true compositions of the samples were refined for the samples with nominal compositions x = 0.12, 0.18, and 0.20. The sample with nominal x = 0.15 was calculated from a linear fit of other three samples. The highest zT value of 0.94 at 420 °C was obtained for a sample of nominal composition $In_{0.18}Co_4Sb_{12}$, which has a true In content of x = 0.160.

room temperature, zT > 0.2, and it increases with increasing temperature up to maximum values (zT_{max}) ranging from 0.75 to 0.94 at 370 and 420 °C, respectively. At higher temperatures the influence of bipolar conduction forces the zT value to decrease again. It is important to note that the sample with the highest figure of merit has a composition $In_{0.18}Co_4Sb_{12}$ (rather than $In_{0.20}Co_4Sb_{12}$ as one might expect). This finding can be easily understood based on the true In content. Rietveld refinement of the synchrotron diffraction data allowed a very precise determination of the sample compositions. As the formation of InSb competes with the formation of $In_xCo_4Sb_{12}$ the sample with a nominal composition $In_{0.18}Co_4Sb_{12}$ has an indium content x = 0.16, while the sample with a nominal composition $In_{0.20}Co_4Sb_{12}$ actually has an In content of x = 0.144.

The In content of the sample with nominal composition of $In_{0.15}Co_4Sb_{12}$ could not be refined properly. As systematic errors (beam instability, absorption, extinction, etc.) can be ruled out, this might be attributed to sample preparation, which is reflected in higher standard deviations. Still, the high-resolution X-ray data show that the lattice parameter a is a very sensitive probe of the In content. It shows the true In filling and predicts the correlated zT values (Figure 10).

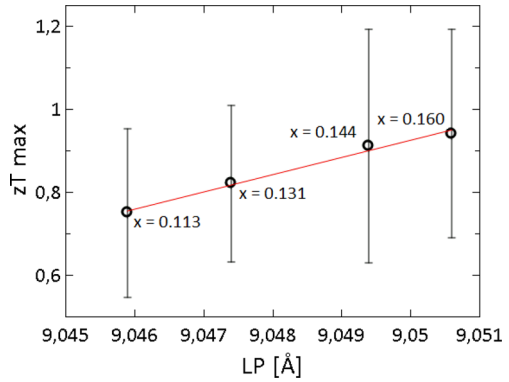

Figure 10. Refined lattice constant plotted versus the measured zT values for nominal compositions $In_xCo_4Sb_{12}$ (x = 0.12, 0.15, 0.18, and 0.20) and the true composition $In_xCo_4Sb_{12}$ (x = 0.113, 0.131, 0.160, and 0.144). The true compositions of the samples were refined for the samples with nominal compositions x = 0.12, 0.18, and 0.20. The sample with nominal x = 0.15 (true 0.131) was calculated from a linear fit of the other three samples.

CONCLUSIONS

A new and facile two-step synthesis was developed to synthesize high-quality phase pure bulk $In_xCo_4Sb_{12}$ skutterudites with nominal compositions x = 0.12, 0.15, 0.18, and 0.20 to study the effect of the interstitial site filling on the structural stability and the thermoelectric properties. Differently from the standard melt−quench−anneal preparation the two-step synthesis separates the kieftite formation from the topotactic filler insertion. This allows not only conducting the reactions at lower temperatures with shorter reaction times, but also circumvents the formation of impurity phases. The procedure can be transferred to other filled skutterudites as well. Current-assisted short-time sintering was used to consolidate the obtained powders into high-density (>98%) pellets for thermoelectric characterization. Structural and microstructural analysis of the obtained powders and consolidated pellets were conducted by SEM/EDX, standard XRD, and ^{121}Sb Mößbauer spectroscopy, which showed the presence of homogeneous, single-phase skutterudite materials with grain sizes at the order of 2−5 μm. The excellent sample homogeneity was demonstrated by PSM measurements of the pellet surfaces, illustrating a homogeneous and narrow distribution of the measured Seebeck values. The current-assisted short-time sintering of the powders and thermal cycling during thermoelectric characterization of consolidated pellets did not have a significant effect on microstructure and phase composition.

The topotactic In insertion, the degree of In filling, and repeated thermal cycling showed no signature in the ^{121}Sb Mößbauer spectra. Although no secondary phases could be detected by SEM/EDX, ^{121}Sb Mößbauer spectroscopy or laboratory XRD, high-resolution synchrotron data revealed a very small volume fraction (~0.1%) of InSb in samples of nominal composition $In_{0.18}Co_4Sb_{12}$ and $In_{0.20}Co_4Sb_{12}$. Rietveld refinements showed a linear correlation between the true In occupancy and the lattice parameter. Proper determination of the lattice parameter can thus be used to extrapolate the true occupancy of filler atoms in skutterudite-type materials, where proper refinements of the interstitial atom occupancy are not possible. A slight decrease in the lattice parameter, correlated with a change in the electronic transport properties after several thermal cycles above 480 °C may indicate a minor degree of

DOI: 10.1021/acs.inorgchem.5b00799
Inorg. Chem. 2015, 54, 7818−7827

material deterioration, which might limit future high-temperature applications.

The very high purity of the In filled skutterudites allowed examining the effect of the true degree of In filling on the transport properties without any bias from side phases. Due to the electron donating nature of the filler atom, the charge carrier concentration scaled with the degree of In filling. This led to an increase of the electrical conductivity and a decrease of the Seebeck coefficient, while the lattice thermal conductivity decreased. The corresponding figure of merit was close to unity at 420 °C for a sample of nominal composition $In_{0.18}Co_4Sb_{12}$. This improvement can be attributed to the insertion of In into the kieftite structure. The presence of InSb side phases in minor amounts had no significant effect on the transport properties. However, the lower true degree of In filling, which is a direct consequence of InSb side phase formation, has a dramatic effect on the thermoelectric properties as demonstrated by the sample of nominal composition $In_{0.20}Co_4Sb_{12}$. The presence of InSb as side phase in amounts as small as ∼0.1 vol% led to a substantially lower degree of interstitial site filling, which can be attributed to the different In content in filled skutterudites and InSb. Due to the lower level of In filling the figure of merit decreased by almost 18%, which demonstrates the importance of the true filler atom content in skutterudite materials. The formation of InSb during the synthesis of $In_xCo_4Sb_{12}$ skutterudites, therefore, plays a crucial role for the true level of In filling.

■ ASSOCIATED CONTENT

Ⓢ Supporting Information

Seebeck distribution measured on both sides of all samples (Figures S1−S8); Mößbauer spectra of $In_xCo_4Sb_{12}$ samples after consolidation and thermal cycling (Figures S9−S13); complete set of refined synchrotron data (Figures S14 and S15 and Tables S1 and S2); electronic contributions to the thermal conductivity (Figures S14 and S15); comparison of the dependence of the refined lattice parameter *a* from the In site occupancy using the data of He et al. (Figure S16); electronic contributions to the thermal conductivity estimated using a single parabolic band model (Figure S17); dependence of lattice thermal conductivity on the degree of In filling for $In_xCo_4Sb_{12}$ (nominal x = 0.12, 0.15, 0.18, and 0.20) (Figure S18); differences in the thermal conductivity for the set of In filled skutterudites $In_xCo_4Sb_{12}$ with a nominal degree x of In filling (x = 0.12, 0.15, 0.18, and 0.20) and a true composition $In_xCo_4Sb_{12}$ (x = 0.113, 0.131, 0.160, and 0.144) (Figure S19). The Supporting Information is available free of charge on the ACS Publications website at DOI: 10.1021/acs.inorgchem.5b00799.

■ AUTHOR INFORMATION

Corresponding Authors

*E-mail: eckhard.muellerdlr.de.

*E-mail: tremel@uni-mainz.de. Fax: +49-6131-39-25605. Phone: +49-6131- 39-25135.

Author Contributions

▽These authors contributed equally.

Notes

The authors declare no competing financial interest.

■ ACKNOWLEDGMENTS

This research was funded by the Deutsche Forschungsgemeinschaft (DFG) through priority program 1386 *Nanostructured Thermoelectrics*. Financial support through the Excellence Initiative (DFG/GSC 266) is acknowledged by C.P.H. We also thank 11-BM beamline staff for the measurements. Use of the Advanced Photon Source at Argonne National Laboratory was supported by the U.S. Department of Energy, Office of Science, Office of Basic Energy Sciences, under Contract No. DE-AC02-06CH11357.

■ REFERENCES

(1) DiSalvo, F. J. *Science* **1999**, *285*, 703−706.
(2) Slack, G. A. In *Handbook of thermoelectrics*; Rowe, D. M., Ed.; CRC Press: Boca Raton, FL, 1995; pp 407−440.
(3) Snyder, G. J.; Toberer, E. S. *Nat. Mater.* **2008**, *7*, 105−114.
(4) Venkatasubramanian, R.; Siivola, E.; Colpitts, T.; O'Quinn, B. *Nature* **2001**, *413*, 597−602.
(5) Harman, T. C.; Taylor, P. J.; Walsh, M. P.; LaForge, B. E. *Science* **2002**, *297*, 2229−2232.
(6) Hsu, K. F.; Loo, S.; Guo, F.; Chen, W.; Dyck, J. S.; Uher, C.; Hogan, T.; Polychroniadis, E. K.; Kanatzidis, M. G. *Science* **2004**, *303*, 818−821.
(7) Poudel, B.; Hao, Q.; Ma, Y.; Lan, Y. C.; Minnich, A.; Yu, B.; Yan, X.; Wang, D. Z.; Muto, A.; Vashaee, D.; Chen, X. Y.; Liu, J. M.; Dresselhaus, M. S.; Chen, G.; Ren, Z. *Science* **2008**, *320*, 634−638.
(8) Zeier, W. G.; LaLonde, A.; Heinrich, C.; Panthöfer, M.; Snyder, G. J.; Tremel, W. *J. Am. Chem. Soc.* **2012**, *134*, 7147−7154.
(9) Sales, B. C.; Mandrus, D.; Williams, R. K. *Science* **1996**, *272*, 1325−1328.
(10) Heremans, J. P.; Jovovic, V.; Toberer, E. S.; Saramat, A.; Kurosaki, K.; Charoenphakdee, A.; Yamanaka, S.; Snyder, G. J. *Science* **2008**, *321*, 554−558.
(11) Zhao, L.-D.; Lo, S.-H.; Zhang, Y.; Sun, H.; Tan, G.; Uher, C.; Wolverton, C.; Dravid, V. P.; Kanatzidis, M. G. *Nature* **2014**, *508*, 373−377.
(12) Nolas, G. S.; Morelli, D. T.; Tritt, T. M. *Annu. Rev. Mater. Sci.* **1999**, *29*, 89−116.
(13) Uher, C. *Semiconductors Semimetals*; Academic Press: San Diego, 2001; Vol. *69*, pp 139−253
(14) Morelli, D. T.; Meisner, G. P. *J. Appl. Phys.* **1995**, *77*, 3777−3781.
(15) Kawaharada, Y.; Kurosaki, K.; Uno, M.; Yamanaka, S. *J. Alloys Compd.* **2001**, *315*, 193−197.
(16) Keppens, V.; Mandrus, D.; Sales, B. C.; Chakoumakos, B. C.; Dai, P.; Coldea, R.; Maple, M. B.; Gajewsk, D. A.; Freeman, E. J.; Bennington, S. *Nature* **1998**, *395*, 876−878.
(17) Schmøkel, M. S.; Bjerk, L.; Overgaard, J.; Larsen, F. K.; Madsen, G. K. H.; Sugimoto, K.; Takata, M.; Ibersen, B. B. *Angew. Chem., Int. Ed.* **2013**, *52*, 1503−1506.
(18) Schmøkel, M. S.; Bjerg, L.; Larsen, F. K.; Overgaard, J.; Cenedese, S.; Christensen, M.; Madsen, G. H. K.; Gatti, C.; Nishibori, E.; Sugimoto, K.; Takata, M.; Ibersen, B. B. *Acta Crystallogr., Sect. A: Found. Crystallogr.* **2013**, *69*, 570−582.
(19) Mi, J.-L.; Christensen, M.; Nishibori, E.; Kuznetsov, V.; Rowe, D. M.; Ibersen, B. B. *J. Appl. Phys.* **2010**, *107*, 113507.
(20) Mi, J.-L.; Christensen, M.; Nishibori, E.; Iversen, B. B. *Phys. Rev. B: Condens. Matter Mater. Phys.* **2011**, *84*, 064114.
(21) Christensen, M.; Iversen, B. B.; Bertini, L.; Toprak, M.; Muhammed, M.; Nishibori, E. *J. Appl. Phys.* **2004**, *96*, 3148−3157.
(22) Jeitschko, W.; Braun, D. *Acta Crystallogr., Sect. B: Struct. Crystallogr. Cryst. Chem.* **1977**, *33*, 3401−3406.
(23) Braun, D. J.; Jeitschko, W. *J. Less-Common Met.* **1980**, *72*, 147−156.
(24) Nolas, G. S.; Cohn, J. L.; Slack, G. A. *Phys. Rev. B: Condens. Matter Mater. Phys.* **1998**, *58*, 164−170.

DOI: 10.1021/acs.inorgchem.5b00799
Inorg. Chem. 2015, 54, 7818−7827

(25) Morelli, D. T.; Meisner, G. P.; Chen, B. X.; Hu, S. Q.; Uher, C. *Phys. Rev. B: Condens. Matter Mater. Phys.* **1997**, *56*, 7376−7383.
(26) Lamberton, G. A.; Bhattacharya, S.; Littleton, R. T.; Kaeser, M. A.; Tedstrom, R. H.; Tritt, T. M.; Yang, J.; Nolas, G. S. *Appl. Phys. Lett.* **2002**, *80*, 598−600.
(27) Kuznetsov, V. L.; Kuznetsova, L. A.; Rowe, D. M. *J. Phys.: Condens. Matter* **2003**, *15*, 5035−5048.
(28) Chen, L. D.; Kawahara, T.; Tang, X. F.; Goto, T.; Hirai, T.; Dyck, J. S.; Chen, W.; Uher, C. *J. Appl. Phys.* **2001**, *90*, 1864−1868.
(29) Puyet, M.; Lenoir, B.; Dauscher, A.; Dehmas, M.; Stiewe, C.; Müller, E. *J. Appl. Phys.* **2004**, *95*, 4852−4855.
(30) Zhao, X. Y.; Shi, X.; Chen, L. D.; Zhang, W. Q.; Zhang, W. B.; Pei, Y. Z. *J. Appl. Phys.* **2006**, *99*, 053711/1−4.
(31) Pei, Y. Z.; Chen, L. D.; Zhang, W.; Shi, X.; Bai, S. W.; Zhao, X. Y.; Mei, Z. G.; Li, X. Y. *Appl. Phys. Lett.* **2006**, *89*, 221107/1−4.
(32) Pei, Y. Z.; Yang, J.; Chen, L. D.; Zhang, W.; Salvador, J. R.; Yang, J. *Appl. Phys. Lett.* **2009**, *95*, 042101/1−3.
(33) Sellinschegg, H.; Stuckmeyer, S. L.; Hornbostel, M. D.; Johnson, D. C. *Chem. Mater.* **1998**, *10*, 1096−1101.
(34) Nolas, G. S.; Takizawa, H.; Endo, T.; Sellinschegg, H.; Johnson, D. C. *Appl. Phys. Lett.* **2000**, *77*, 52−54.
(35) Nolas, G. S.; Yang, J.; Takizawa, H. *Appl. Phys. Lett.* **2004**, *84*, 5210−5212.
(36) Liang, Y.; Borrmann, H.; Baenitz, M.; Schnelle, W.; Budnyk, S.; Zhao, J. T.; Grin, Yu. *Inorg. Chem.* **2008**, *47*, 9489−9496.
(37) Fukuoka, H.; Yamanaka, S. *Chem. Mater.* **2010**, *22*, 47−51.
(38) Tang, Y.; Qiu, Y.; Xi, L.; Shi, X.; Zhang, W.; Chen, L.; Tseng, S.-M.; Chen, S.-W.; Snyder, G. J. *Energy Environ. Sci.* **2014**, *7*, 812−819.
(39) Shi, X.; Yang, J.; Salvador, J. R.; Chi, M.; Cho, J. Y.; Wang, H.; Bai, S.; Yang, J.; Zhang, W.; Chen, L. *J. Am. Chem. Soc.* **2011**, *133*, 7837−7846.
(40) Hermann, R. P.; Jin, R. J.; Schweika, W.; Grandjean, F.; Mandrus, D.; Sales, B. C.; Long, G. J. *Phys. Rev. Lett.* **2003**, *90*, 135505/1−4.
(41) Shi, X.; Kong, H.; Li, C.-P; Uher, C.; Yang, J.; Salvador, J.; Wang, H.; Chen, L.; Zhang, W. *Appl. Phys. Lett.* **2008**, *92*, 182101/1−3.
(42) Rogl, G.; Grytsiv, A.; Rogl, P.; Peranio, N.; Bauer, E.; Zehetbauer, M.; Eibl, O. *Acta Mater.* **2014**, *63*, 30−43.
(43) Xi, L.; Yang, J.; Lu, C.; Mei, Z.; Zhang, W.; Chen, L. *Chem. Mater.* **2010**, *22*, 2384−2394.
(44) Toprak, M. S.; Stiewe, C.; Platzek, D.; Williams, S.; Bertini, L.; Müller, E.; Gatti, C.; Zhang, Y.; Rowe, M.; Muhammed, M. *Adv. Funct. Mater.* **2004**, *14*, 1189−1196.
(45) Li, H.; Tang, X.; Zhang, Q.; Uher, C. *Appl. Phys. Lett.* **2009**, *94*, 102114/1−3.
(46) Li, X.; Chen, L.; Fan, J.; Zhang, W.; Kawahara, T.; Hirai, T. *J. Appl. Phys.* **2005**, *98*, 083702/1−7.
(47) Liu, W.-S.; Zhang, B.-P; Li, J.-F.; Zhang, H.-L.; Zhao, L.-D. *J. Appl. Phys.* **2007**, *102*, 103717/1−8.
(48) Yang, J.; Chen, Y.; Zhu, W.; Peng, J.; Bao, S.; Fan, X. A.; Duan, X. *J. Solid State Chem.* **2006**, *179*, 212−216.
(49) Li, Q.; Lin, Z.; Zhou, J. *J. Electron. Mater.* **2009**, *38*, 1268−1272.
(50) Biswas, K.; Muir, S.; Subramanian, M. *Mater. Res. Bull.* **2011**, *46*, 2288−2290.
(51) Liang, T.; Su, X.; Yan, Y.; Zheng, G.; Zhang, Q.; Chi, H.; Tang, X.; Uher, C. *J. Mater. Chem. A* **2014**, *2*, 17914−17918.
(52) Zhang, J.; Xu, B.; Wang, L.-M.; Yu, D.; Yang, J.; Yu, F.; Liu, Z.; He, J.; Wen, B.; Tian, Y. *Acta Mater.* **2012**, *60*, 1246−1251.
(53) Liu, W.-S.; Zhang, B.-P; Li, J.-F; Zhao, L.-D. *J. Phys. D: Appl. Phys.* **2007**, *40*, 566−572.
(54) Okamoto, H. *J. Phase Equilib. Diffus.* **2005**, *26*, 198.
(55) Sesselmann, A. J. Ph.D. Dissertation, Universität Augsburg, 2012.
(56) Liu, W.-S.; Zhang, B.-P.; Li, J.-F; Zhao, L.-D. *J. Phys. D: Appl. Phys.* **2007**, *40*, 6784−6790.
(57) He, T.; Chen, J.; Rosenfeld, H. D.; Subramanian, M. A. *Chem. Mater.* **2006**, *18*, 759−762.
(58) Du, Y.; Cai, K. F.; Chen, S.; Qin, Z.; Shen, S. Z. *J. Electron. Mater.* **2011**, *40*, 1215−1220.
(59) Li, G.; Kurosaki, K.; Ohishi, Y.; Muta, H.; Yamanaka, S. *J. Electron. Mater.* **2013**, *42*, 1463−1468.
(60) Sesselmann, A. J.; Dasgupta, T.; Kelm, K.; Müller, E.; Perlt, S.; Zastrow, S. *J. Mater. Res.* **2011**, *26*, 1820−1826.
(61) Sharp, J. W.; Jones, E. C.; Williams, R. K.; Martin, P. M.; Sales, B. C. *J. Appl. Phys.* **1995**, *78*, 1013−1018.
(62) Smalley, A. L. E.; Kim, S.; Johnson, D. C. *Chem. Mater.* **2003**, *15*, 3847−3851.
(63) Coelho, A. *Topas Academic*, Version 4.1; Coelho Software, Brisbane, 2007.
(64) Cheary, V.; Coelho, A. *J. Appl. Crystallogr.* **1992**, *25*, 109−121.
(65) de Boor, J.; Stiewe, C.; Ziolkowski, P.; Dasgupta, T.; Karpinski, G.; Lenz, E.; Edler, F.; Müller, E. *J. Electron. Mater.* **2013**, *42*, 1711−1718.
(66) de Boor, J.; Müller, E. *Rev. Sci. Instrum.* **2013**, *84*, 065102.
(67) Platzek, D.; Karpinski, G.; Drasar, C.; Müller, E. *Mater. Sci. Forum* **2005**, *492*−*493*, 587−592.
(68) Ishida, K.; Nishizawa, T. *J. Phase Equilib.* **1990**, *11* (3), 243−248.
(69) Lu, Z. Q. J.; Lowhorn, N. D.; Wong-Ng, W.; Zhang, W.; Thomas, E. L.; Otani, M.; Green, M. L.; Tran, T. N.; Dilley, N. R.; Downey, A.; Edwards, B.; Elsner, N.; Ghamaty, S.; Hogan, T.; Jie, Q.; Li, Q.; Martin, J.; Nolas, G.; Obara, H.; Sharp, J.; Venkatasubramanian, R.; Willigan, R.; Yang, J.; Tritt, T. *J. Res. Natl. Inst. Stand. Technol.* **2009**, *114*, 37−55.
(70) Kjekshus, A.; Nicholson, D. G.; Rakke, T.; Jalonen, H.; Lüning, B.; Swahn, C. G. *Acta Chem. Scand.* **1973**, *27*, 1315−1320.
(71) Lefebvre-Devos, I.; Lassalle, M.; Wallart, X.; Olivier-Fourcade, J.; Monconduit, L.; Jumas, J. *Phys. Rev. B: Condens. Matter Mater. Phys.* **2001**, *63*, 125110/1−7.
(72) Devos, I.; Womes, M.; Heilemann, M.; Olivier-Fourcade, J.; Jumas, J.-C.; Tirado, J.-L. *J. Mater. Chem.* **2004**, *14*, 1759−1767.
(73) Figueirêdoa, C. A.; Gallasa, M. R.; Zorzic, E.; Perottonia, C. A. *J. Alloys Compd.* **2014**, *598*, 266−271.
(74) Grytsiv, A.; Rogl, P.; Michor, H.; Bauer, E.; Giester, G. *J. Electron. Mater.* **2013**, *42*, 2940−2952.
(75) Tang, Y.; Qiu, Y.; Xi, L.; Shi, X.; Zhang, W.; Chen, L.; Tseng, S.-M.; Chen, S. W.; Snyder, G. J. *Energy Environ. Sci.* **2014**, *7*, 812−819.
(76) Jeitschko, W.; Foecker, A. J.; Paschke, D.; Dewalsky, M. V.; Evers, C. B. H.; Künnen, B.; Lang, A.; Kotzyba, G.; Rodewald, U.; Möller, M. H. *Z. Anorg. Allg. Chem.* **2000**, *626*, 1112−1120.

DOI: 10.1021/acs.inorgchem.5b00799
Inorg. Chem. 2015, 54, 7818−7827